Computational Study of the Effect of Dispersion Interactions on the Thermochemistry of Aggregation of Fused Polycyclic Aromatic Hydrocarbons as Model Asphaltene Compounds in Soluti...

ARTICLE *in* THE JOURNAL OF PHYSICAL CHEMISTRY A · JANUARY 2014

Impact Factor: 2.69 · DOI: 10.1021/jp408005h · Source: PubMed

6 AUTHORS, INCLUDING:

Stanislav R. Stoyanov
University of Alberta
44 PUBLICATIONS **764** CITATIONS
SEE PROFILE

Sergey Gusarov
National Research Council Canada
66 PUBLICATIONS **842** CITATIONS
SEE PROFILE

José Walkimar de M. Carneiro
Universidade Federal Fluminense
115 PUBLICATIONS **1,422** CITATIONS
SEE PROFILE

THE JOURNAL OF PHYSICAL CHEMISTRY A

Article

pubs.acs.org/JPCA

Computational Study of the Effect of Dispersion Interactions on the Thermochemistry of Aggregation of Fused Polycyclic Aromatic Hydrocarbons as Model Asphaltene Compounds in Solution

Leonardo Moreira da Costa,[†,‡,§,∥] Stanislav R. Stoyanov,[†,⊥] Sergey Gusarov,[†] Peter R. Seidl,[‡] José Walkimar de M. Carneiro,*[,§] and Andriy Kovalenko*[,†,#]

[†]National Institute for Nanotechnology, National Research Council of Canada, 11421 Saskatchewan Drive, Edmonton, Alberta T6G 2M9, Canada

[‡]Department of Organic Processes, School of Chemistry, Universidade Federal do Rio de Janeiro, Rio de Janeiro, RJ 21941-901, Brazil

[§]Institute of Chemistry, Universidade Federal Fluminense, Niteroi, RJ 24220-900, Brazil

[∥]Centro Universitário da Zona Oeste, Avenida Manuel Caldeira de Alvarenga 1203, Campo Grande, RJ 23070-200, Brazil

[⊥]Department of Chemical and Materials Engineering, University of Alberta, Edmonton, Alberta T6G 2V4, Canada

[#]Department of Mechanical Engineering, University of Alberta, Edmonton, Alberta T6G 2G8, Canada

Supporting Information

ABSTRACT: Density functional theory (DFT), Møller−Plesset second-order perturbation theory (MP2), and semiempirical methods are employed for the geometry optimization and thermochemistry analysis of $\pi-\pi$ stacked di-, tri-, tetra-, and pentamer aggregates of the fused polycyclic aromatic hydrocarbons (PAHs) naphthalene, anthracene, phenanthrene, tetracene, pyrene, and coronene as well as benzene. These aggregates (stabilized by dispersion interactions) are highly relevant to the intermolecular aggregation of asphaltenes, major components of heavy petroleum. The strength of $\pi-\pi$ stacking interaction is evaluated with respect to the π-stacking distance and thermochemistry results, such as aggregation enthalpies, entropies, and Gibbs free energies (ΔG^{298}). For both π-stacking interplanar distances and thermochemistry, the ωB97X-D functional with an augmented damped R^{-6} dispersion correction term and MP2 are in the closest agreement with the highly accurate spin-component scaled MP2 (SCS-MP2) method that we selected as a reference. The ΔG^{298} values indicate that the aggregation of coronene is spontaneous at 298 K and the formation of pyrene dimers occurs spontaneously at temperature lower than 250 K. Aggregates of smaller PAHs would be stable at even lower temperature. These findings are supported by X-ray crystallographic determination results showing that among the PAHs studied only coronene forms continuous stacked aggregates in single crystals, pyrene forms dimers, and smaller PAHs do not form $\pi-\pi$ stacked aggregates. Thermochemistry analysis results show that PAHs containing more than four fused benzene rings would spontaneously form aggregates at 298 K. Also, round-shaped PAHs, such as phenanthrene and pyrene, form more stable aggregates than linear PAHs, such as anthracene and tetracene, due to decreased entropic penalty. These results are intended to help guide the synthesis of model asphaltene compounds for spectroscopic studies so as to help understand the aggregation behavior of heavy petroleum.

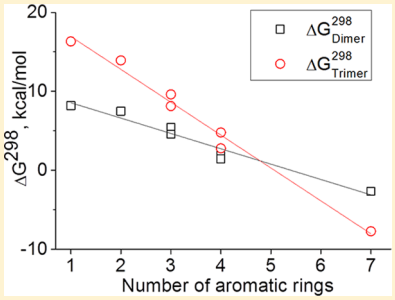

INTRODUCTION

Dispersion interactions (ubiquitous throughout highly polarizable organic molecules) play key roles in crystal engineering, molecular recognition and biological processes and are a subject of continuous interest in science.[1−7] For example, these interactions are important in the $\pi-\pi$ stacking of nucleotides that form the 3D helicoidal structure of DNA,[8] microscopic organization of graphene sheets increasing its hardness,[9] molecular signalization for drug-receptor binding,[10] and formation of chemical scaling deposits that drastically decrease petroleum recovery.[11] Although dispersion interactions are very important in all these chemical and biological processes, the accurate theoretical description of these interactions remains a difficult task.[12−15] Among the several components contributing to intermolecular interactions, the dispersion energy is the most challenging for the quantum mechanical methods to incorporate in a reliable and computationally efficient manner.[12] This interaction, also known as the London force, has its origin in molecular polarization and electron correlation. Thus, high level treatment of electron correlation using an extended atomic orbital basis set is necessary for the accurate and correct description of dispersion.[11,12] Even simple systems, such as the benzene dimer, can be extremely challenging for the most robust quantum mechanical methods.[16,17]

Received: August 9, 2013
Revised: December 16, 2013
Published: January 16, 2014

   dx.doi.org/10.1021/jp408005h | J. Phys. Chem. A 2014, 118, 896−908

The majority of the standard semiempirical, density functional theory (DFT), and ab initio methods does not properly account for the dispersion term. The classical, semiempirical, and Hartree−Fock[18−20] methods do not evaluate dispersion forces in the electronic structure calculation.[11] Standard DFT functionals with local exchange−correlation overestimate[21] binding energies of weakly bound systems, whereas with nonlocal exchange−correlation the binding energies are underestimated.[22] The Møller−Plesset second-order perturbation theory (MP2)[23−27] overestimates[28,29] the dispersion energy, especially in systems containing delocalized π-electrons, whereas the coupled cluster with single and double excitations (CCSD)[30] method usually underestimates it and requires the inclusion of a perturbative triple states correction to quantitatively reproduce the interaction energy.[21,31] Several dispersion-corrected methods have been proposed to remedy the deficiency in the description of the London dispersion forces. The inclusion of an augmented damped R^{-6} dispersion term (DFT-D)[32] or C atom-centered dispersion-correcting potentials (DFT-DCP)[33,34] in the traditional DFT have been presented as effective approaches to describe London forces without increasing the computational cost. The DFT-D functional with empirical atom−atom dispersion corrections ωB97X-D has been shown to perform very well for covalent and noncovalent interactions as well as thermochemistry.[35,36] The performance of DFT-DCP has not been thoroughly evaluated with respect to thermochemistry.[28] The augmented damped R^{-6} dispersion term has also been parametrized to reproduce the benchmark coupled-cluster with single and double and perturbative triple excitations (CCSD(T)) interaction energies and included in the semiempirical level originating the PM6-DH2 method.[37] The spin component scaled (SCS) methods (SCS-MP2[38,39] and SCS-CCSD[31]), based on a separate scaling of the correlation energy contributions from antiparallel-spin ($\alpha\beta$, "singlet") and parallel-spin ($\alpha\alpha$, $\beta\beta$, "triplet") pairs of electrons, drastically increase the accuracy of the dispersion energy calculation. The SCS-MP2 method has been further parametrized to represent noncovalent interaction energies of dimers in nucleic acids (SCSN-MP2)[40] and for molecular interaction (MI) abbreviated as SCS(MI)-MP2.[41] Other methods, such as the time-dependent (TD) coupled-perturbed DFT[42] and the combination of DFT with the symmetry-adapted intermolecular perturbation theory[43−45] (SAPT) are also implemented, albeit with a rather high computational cost.

The consideration of dispersion interactions is extremely important for theoretical studies of molecules with large π-electronic systems, such as asphaltenes. Asphaltenes (the densest fraction of petroleum) are a complex mixture of heavy organic molecules containing fused polycyclic aromatic hydrocarbons (PAH), pendant alkyl chains and polar functional groups with O, N, and S atoms.[10] According to our current understanding, asphaltenes have two main types of macrostructural arrangements, as shown in Figure 1. The continental model[46] is based on a core aromatic moiety containing more than seven fused rings covalently bonded to aliphatic groups. The archipelago model,[47] supported by chemical and thermal degradation studies,[48] is based on smaller aromatic groups linked by aliphatic tethers. Experimental[49,50] and theoretical[51−55] studies have shown that asphaltenes have a strong tendency to associate and originate insoluble aggregates that drastically decrease oil recovery and transport efficiency. In asphaltene aggregation, the solvent media where the organic

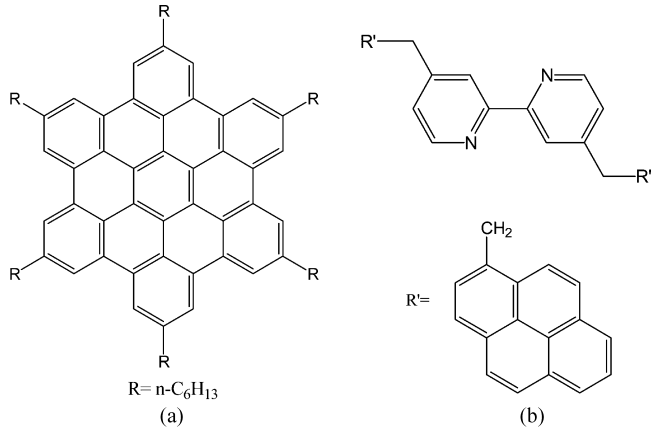

Figure 1. Macrostructural models of asphaltene molecules. (a) Hexabenzocoronene is an example of a continental model of asphaltene. (b) 4,4′-Bis(2-pyren-1-ylethyl)-2,2′-bipyridine[37,38,42,43] is an example of an archipelago model of asphaltene.

molecules are dispersed affects the magnitude of the intermolecular interactions through solute−solvent intermolecular interactions.[39,40] According to the supramolecular assembly model for asphaltene aggregation recently proposed by Gray et al., the driving forces that promote asphaltene aggregation are due to cooperative binding by hydrogen bonding, $\pi-\pi$ stacking, acid−base interactions, and metal coordination as well as formation of hydrophobic pockets, porous networks, and host−guest complexes.[56] Several molecular mechanics and molecular dynamics studies have shown that due to the large conjugated π-electronic system, the dispersion interaction is fundamental to the strength of the aggregation interaction among asphaltene molecules.[39,40] Recently, we reported that aggregates of asphaltene model compounds containing pyridine and PAH moieties are greatly stabilized by both hydrogen bonding to water bridges from solvent and dispersion interactions, as studied using the ωB97X-D functional with dispersion correction and the conductor-like polarizable continuum model (CPCM) of solvation.[57,58] These water bridges form in chloroform solvent containing traces of water and cause a decrease of the solvation free energy for aggregation,[42,43] as predicted using the statistical-mechanical three-dimensional reference interaction site model molecular theory of solvation with the Kovalenko−Hirata closure approximation (3D-RISM-KH).[59−62] The effects of hydrogen bonding and dispersion interaction on supramolecular aggregation in solution are investigated on the basis of the enthalpy and Gibbs free energy (ΔG^{298}) of aggregation, and the results are validated with respect to experimental ^{1}H NMR spectra.[42,43]

In this work, we employ MP2 as well as DFT and semiempirical methods with dispersion corrections to study the homodimerization, trimerization, tetramerization, and pentamerization of the series of PAHs benzene, naphthalene, anthracene, phenanthrene, tetracene, pyrene, and coronene that are constitutive blocks of model asphaltene compounds.[38] We evaluate the ability of DFT functionals with different types of dispersion interaction corrections to predict the optimized geometry and thermochemistry of aggregation with respect to the highly accurate SCS-MP2 method, selected as a reference method, as well as structural information from experiment. In view of the recent statements by Grimme et al. that the SCS(MI)-MP2 and SCSN-PM2 parametrizations have no

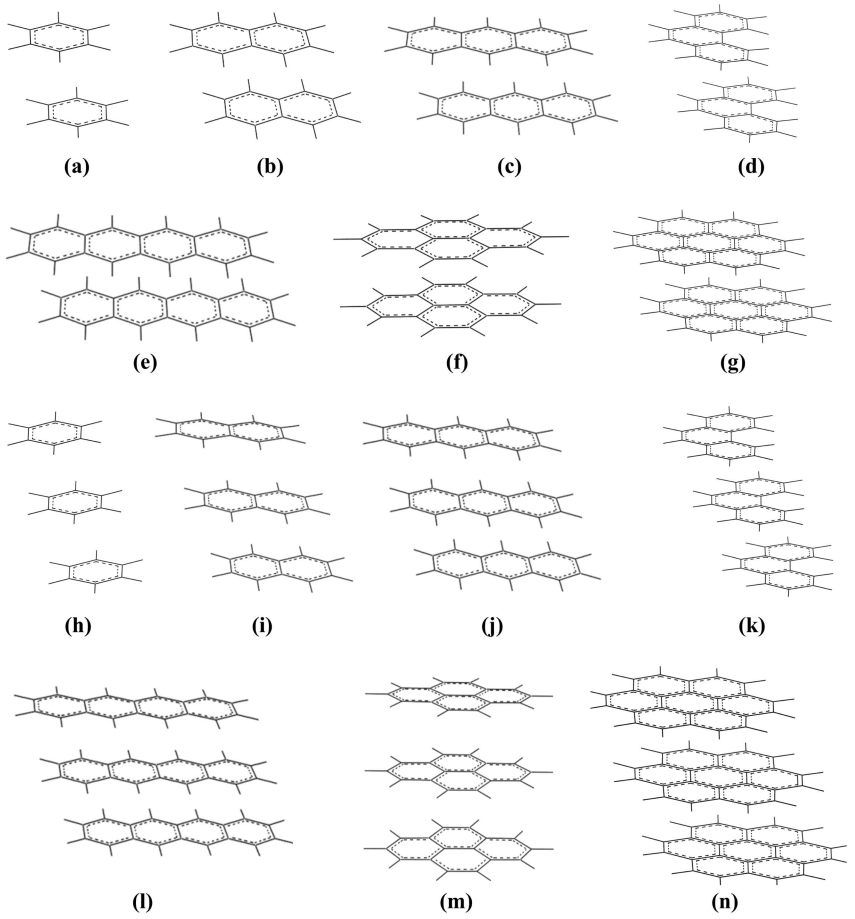

Figure 2. Optimized ωB97X-D/6-31+G(d,p) aggregate structures (dimer and trimer) of benzene (a and h), naphthalene (b and i), anthracene (c and j), phenanthrene (d and k), tetracene (e and l), pyrene (f and m), and coronene (g and n), respectively.

physical interpretations and according to the present understanding have no reasonable explanation in terms of the corresponding wave functions,[63] we restrained from using these methods at this stage.

Moreover, we explore the effect of PAH size and shape as well as the interplay between enthalpy and entropy on the spontaneity of $\pi-\pi$ stacking aggregation.

COMPUTATIONAL TECHNIQUE

The MP2[20] and DFT calculations were performed using the Gaussian 09 computational chemistry software.[64] For the DFT calculations, we employed universal hybrid functionals, such as the Becke's three-parameter exchange and Lee, Yang, and Parr correlation (B3LYP)[65,66] and Perdew, Burke, and Ernzerhof (PBE, also known as PBE0PBE),[67,68] long-range interaction corrected hybrid functionals, such as CAM-B3LYP[69] and LC-wPBE[70−73] functionals, and hybrid functionals with both dispersion and long-range interaction corrections, such as B97D[25,27,74] and ωB97X-D,[25,27] as well as the B3LYP functional with C atom-centered dispersion-correcting potentials B3LYP-DCP.[26] The B97D3 functional, which includes the D3 version of Grimme's damping function (D3BJ) for dispersion correction[75] and the M06-2X hybrid functional of Zhao and Truhlar[76] were also employed. The spin-component scaled MP2 (SCS-MP2[30]) calculations were performed using the ORCA computational chemistry software.[77] The all-electron 6-31+G(d,p) basis set[78,79] was used for all quantum chemistry calculations. This basis set is recommended specifically for use with the B3LYP-DCP functional.[26b] A grid of 75 radial shells and 302 angular points per shell is used for numerical integrations of the two-electron integrals and their derivatives. All energies listed include corrections for the zero-point energy (ZPE) and basis set superposition error (BSSE). The semiempirical AM1,[80] PM3,[81] PM6,[82] and PM6-DH2 calculations were performed using the MOPAC 2009 software.[83] The effect of chloroform solvent is accounted using the conductor-like polarizable continuum model (CPCM).[84,85]

RESULTS AND DISCUSSION

The geometries of the monomers, homodimers, homotrimers, homotetramers, and homopentamers of the seven PAH compounds included in this study were fully optimized using the uncorrected and dispersion-corrected DFT and semi-empirical as well as MP2 methods. After geometry optimization using these quantum-mechanical methods, the second-order force constant matrix was calculated to confirm the optimized geometry as a genuine minimum on the potential energy surface. The starting structures for the geometry optimization in the dimers, trimers (abc model), tetramers, and pentamers have parallel displaced configurations, which are the most stable for almost all compounds, according to previous computational studies.[15,16] In this model, the molecules are organized in parallel planes with C_2 symmetry, an initial interplanar distance of 3.4 Å, and a horizontal displacement of 0.8 Å between the centers of consecutive aromatic rings of each plane. These

dx.doi.org/10.1021/jp408005h | J. Phys. Chem. A 2014, 118, 896−908

Table 1. Interplanar Distances (Å) for the Dimers, Trimers, Tetramers, and Pentamers of Benzene (Ben), Naphthalene (Naph), Anthracene (Ant), Phenanthrene (Phen), Tetracene (Tet), Pyrene (Pyr), and Coronene (Cor) in the Gas Phase[a]

	PM6-DH2	B3LYP-DCP	B97D	ωB97X-D	MP2	SCS-MP2	exp
			Dimers				
Ben_2	3.46	3.33 (3.33)	3.49 (3.49)	3.45 (3.44)	3.39	3.43	[b]
$Naph_2$	3.44	3.29 (3.29)	3.47 (3.47)	3.44 (3.44)	3.34	3.42	[b]
Ant_2	3.37	3.27 (3.27)	3.46 (3.49)	3.41 (3.44)	3.30		[b]
$Phen_2$	3.37	3.21 (3.21)	3.35 (3.33)	3.37 (3.37)			[b]
Tet_2	3.35	3.26 (3.26)	3.44 (3.44)	3.40 (3.44)	3.28		[b]
Pyr_2	3.34	3.20 (3.18)	3.32 (3.32)	3.34 (3.38)	3.20		3.59[c]
Cor_2	3.37	3.18 (3.18)	3.32 (3.32)	3.38 (3.38)			3.46[d]
			Trimers				
Ben_3	3.44	3.32 (3.36)	3.46 (3.85)	3.44 (3.43)	3.35	3.40	
$Naph_3$	3.39	3.29 (3.30)	3.45 (3.45)	3.43 (3.45)	3.29		
Ant_3	3.37	3.26 (3.27)	3.45 (3.49)	3.40 (3.44)	3.26		
$Phen_3$	3.34	3.21 (3.22)	3.32 (3.33)	3.37 (3.37)			
Tet_3	3.34	3.25 (3.27)	3.40 (3.42)	3.39 (3.43)	3.24		
Pyr_3	3.32	3.19 (3.19)	3.30 (3.32)	3.32 (3.38)	3.15		
Cor_3	3.36	3.17 (3.17)	3.30 (3.31)	3.38 (3.39)			3.46[d]
			Tetramers				
Ben_4	3.40[b]	3.50	3.50	3.50			
$Naph_4$	3.37[b]	3.31	3.31	3.42			
Ant_4	3.44	3.28	3.43	3.44			
$Phen_4$	3.37	3.21	3.28	3.36			
			Pentamers				
Ben_5	3.42[b]	3.49	3.49	3.49			
$Naph_5$	3.38[b]	3.28	3.45	3.45			
Ant_5	3.44	3.27	3.44	3.44			
$Phen_5$	3.34	3.21	3.29	3.35			

[a]The results in chloroform solvent modeled using CPCM are listed in parentheses. [b]Misaligned stacks. [c]Reference 61. [d]Reference 62.

initial geometry parameters have been adopted based on previous studies of optimized asphaltene structures.[39,40]

Geometry Optimization. In Figure 2, we present the structures of the dimers, trimers, tetramers and pentamers for the seven PAHs optimized using the ωB97X-D/6-31+G(d,p) method. In each optimized aggregate, the planes are displaced horizontally so that the center of each benzene ring is essentially above a carbon atom of the neighboring sheet, in agreement with previous studies using the parallel displaced model.[4,12,26] Analogous structures are obtained with all the dispersion-corrected methods. The methods without a dispersion energy correction (B3LYP, PBE, CAM-B3LYP, LC-WPBE, AM1, PM3, and PM6) did not locate any stationary minimum energy structure with parallel planes characteristic of π−π stacking interactions.

In Table 1, we list the π−π stacking interaction distances between the planes in the optimized structures of the dimers, trimers, tetramers, and pentamers calculated using two types of dispersion-corrected density functionals (with augmented damped R^{-6} dispersion correction (B97D and ωB97X-D) and with one-electron correction (B3LYP-DCP)) as well as MP2, SCS-MP2, and the semiempirical PM6-DH2 method. The π−π stacking interaction distances are measured between the best-fitted planes defined by all atoms of each respective monomer of the aggregate. For all the PAHs aggregates, the π−π stacking interaction distances decrease as the number of fused rings increases, as calculated using almost all methods, in a general agreement with previous studies.[7,26] The π−π stacking interaction distances calculated using the PM6-DH2, B97D, and ωB97X-D methods are longer than those of the reference SCS-MP2 method, whereas the B3LYP-DCP and MP2 methods predict shorter distances for both dimers and trimers, also in agreement with previous studies.[2,6,13,86] The M06-2X functional yields shorter interplanar distances than the reference SCS-MP2 and the B97D3 functional agrees with SCS-MP2 (Supporting Information Table S1). The interplanar distances calculated using the ωB97X-D functional are in the best agreement with the reference SCS-MP2 result. Comparison of the dimer and trimer distances allows one to clearly differentiate between two distinct groups of PAHs: linear, with all the benzene rings fused linearly (benzene, naphthalene, anthracene, and tetracene) and round, with the benzene rings fused to form a rather round structure (phenanthrene, pyrene, and coronene). The round aggregates pyrene and coronene are carbon-rich (have higher carbon to hydrogen ratio than linear analogs) and are commonly present in petroleum asphaltenes. The interplanar distances of the round aggregates are shorter than those of the linear aggregates with the same number of benzene rings. It is important to note that as the number of PAHs stacked together is increased, the interplanar distances decrease slightly. In the trimers, the two interplanar distances are systematically equal or shorter (by less than 0.02 Å) than the corresponding distances in the dimers, indicating that the third aromatic sheet has only a marginal influence on the interaction between the first and the second sheet. Similar results are calculated for the tetramer and pentamer aggregates.

The π−π stacking interaction distance optimized using the ωB97X-D functional is in the best agreement with that predicted by the reference SCS-MP2 method, with deviations of 0.02 Å for Ben_2, 0.02 Å for the $Naph_2$, and 0.04 Å for Ben_3, followed by the B97D with deviations of 0.06, 0.05, and 0.06 Å, respectively. Although these DFT-D functionals overestimate

dx.doi.org/10.1021/jp408005h | J. Phys. Chem. A 2014, 118, 896−908

Table 2. Dispersion Interaction Enthalpy (ΔH) in kcal·mol^{-1} (Eq 1) for the Dimers, Trimers, Tetramers, and Pentamers of the Benzene (Ben), Naphthalene (Naph), Anthracene (Ant), Phenanthrene (Phen), Tetracene (Tet), Pyrene (Pyr), and Coronene (Cor) in the Gas Phase[a]

	PM6-DH2	B3LYP-DCP	B97D	ωB97X-D	MP2	SCS-MP2
			Dimers			
Ben_2	−3.61	−1.75 (−1.24)	−2.48 (−2.27)	−2.66 (−2.28)	−2.39	−2.11
$Naph_2$	−7.17	−4.12 (−3.87)	−4.63 (−4.24)	−5.08 (−4.90)	−4.52	−4.21
Ant_2	−11.55	−7.78 (−7.59)	−7.66 (−7.36)	−9.95 (−9.31)		
$Phen_2$	−10.57	−7.21 (−6.88)	−6.82 (−6.22)	−8.95 (−8.14)		
Tet_2	−13.40	−10.70 (−10.49)	−10.81 (−10.12)	−13.08 (−12.56)		
Pyr_2	−12.76	−10.40 (−9.49)	−9.60 (−8.99)	−12.54 (−11.67)		
Cor_2	−22.39	−20.61 (−18.90)	−23.23 (−17.73)	−24.34 (−21.98)		
			Trimers			
Ben_3	−6.95	−2.75 (−2.29)	−3.89 (−2.52)	−5.47 (−5.28)	−4.60	−4.35
$Naph_3$	−11.06	−9.07 (−8.18)	−9.65 (−8.17)	−12.20 (−11.75)		
Ant_3	−22.52	−14.43 (−13.37	−15.88 (−13.90)	−20.42 (−18.17)		
$Phen_3$	−20.49	−11.98 (−12.36)	−13.85 (−13.95)	−17.68 (−17.41)		
Tet_3	−30.27	−20.79 (−20.13)	−22.07 (−20.14)	−25.44 (−24.72)		
Pyr_3	−27.21	−18.70 (−18.38)	−21.31 (−18.16)	−21.62 (−20.67)		
Cor_3	−45.57	−43.41 (−30.69)	−47.58 (−28.10)	−49.41 (−48.83)		
			Tetramers			
Ben_4	−10.95	−4.23	−5.10	−7.02		
$Naph_4$	−22.53	−17.83	−20.15	−23.94		
Ant_4	−38.37	−30.57	−32.62	−36.66		
$Phen_4$	−34.94	−25.54	−26.18	−33.91		
			Pentamers			
Ben_5	−14.60	−6.28	−8.45	−12.28		
$Naph_5$	−29.50	−23.49	−25.95	−30.24		
Ant_5	−47.68	−41.03	−43.82	−49.15		
$Phen_5$	−41.24	−34.67	−35.77	−42.23		

[a]The results in chloroform solvent modeled using CPCM are listed in parentheses.

the interplanar distance, the MP2 method underestimates it with deviations of −0.04, −0.08, and −0.05 Å for Ben_2, $Naph_2$, and Ben_3, respectively, relative to the SCS-MP2 results. The B3LYP-DCP functional predicts significantly shorter interplanar distances, with deviations of −0.10, −0.13, and −0.08 Å for Ben_2, $Naph_2$, and Ben_3, respectively, relative to the SCS-MP2. The semiempirical PM6-DH2 method yields good results for dimers and trimers, with deviations of 0.03, 0.02, and 0.04 Å, for Ben_2, $Naph_2$, and Ben_3, respectively, relative to the SCS-MP2 results but gives structurally distorted stacks for aggregates containing more than three monomers (Table 1, note a).

X-ray crystallographic determinations for the PAHs included in this study show that only pyrene and coronene form $\pi-\pi$ stacked aggregates in the solid state.[87−93] Pyrene forms dimers with interplanar distance of 3.59 Å.[61] Coronene forms infinitely long $\pi-\pi$ stacked aggregates with an interplanar distance of 3.46 Å.[62] The coronene $\pi-\pi$ stacking distance of 3.38 Å optimized using the ωB97X-D functional is in the closest agreement with the coronene crystal structure determination result. The experimentally measured interplanar distances in pyrene and coronene are longer than the calculated ones due to crystal packing.

Effect of Chloroform Solvent on Interplanar Distance. In Table 1, in parentheses we list the interplanar distances for the aggregates optimized in chloroform solvent using the CPCM solvation model and the three dispersion-corrected functionals. The optimized interplanar distances in chloroform tend to be longer than those in the gas phase as solvation weakens the stacking interaction. The largest interplanar distance elongations are obtained for the small PAHs, such as benzene, due to the weak π-stacking forces. We selected chloroform because it is the solvent of choice in spectroscopic studies of asphaltene aggregation, as it has no specific interactions with PAHs and does not interfere with ^{1}H NMR measurements used to study aggregation.[37,38,43]

Thermochemistry of π-Stacking Interactions. In Tables 2−4, we list the changes in enthalpy (ΔH), entropy (ΔS), and Gibbs free energy (ΔG^{298}) for π-stacking interaction among the PAH monomers for di-, tri-, tetra- and pentamerization the aggregates relative to the isolated monomers, calculated according to eqs 1−3:

$$\Delta H = \Delta H_{\mathrm{AGGREGATE}} - m\Delta H_{\mathrm{MONOMER}} \quad (1)$$

$$\Delta S = \Delta S_{\mathrm{AGGREGATE}} - m\Delta S_{\mathrm{MONOMER}} \quad (2)$$

$$\Delta G^{298} = \Delta G^{298}_{\mathrm{AGGREGATE}} - m\Delta G^{298}_{\mathrm{MONOMER}} \quad (3)$$

where m = 2, 3, 4, and 5 for dimers, trimers, tetramers, and pentamers, respectively. These thermodynamic terms are calculated in the gas phase as well as in chloroform solvent accounted using the CPCM continuum solvation model.

Enthalpy Analysis. The dispersion interaction enthalpy values listed in Table 2 show increasing aggregation strength (more negative values) as the aromatic system size is increased, in agreement with previous computational results,[7,26] in the order benzene < naphthalene < phenanthrene < anthracene < pyrene < tetracene < coronene. This trend is observed for all PAH oligomers. The PM6-DH2, ωB97X-D, B97D, and MP2 methods yield more negative interaction enthalpies than the

dx.doi.org/10.1021/jp408005h | J. Phys. Chem. A 2014, 118, 896−908

Table 3. Dispersion Interaction Entropy (ΔS) in cal·mol^{-1} (Eq 2) for the Dimers, Trimers, Tetramers, and Pentamers of the Benzene (Ben), Naphthalene (Naph), Anthracene (Ant), Phenanthrene (Phen), Tetracene (Tet), Pyrene (Pyr), and Coronene (Cor) in the Gas Phase[a]

	B3LYP-DCP	B97D	ωB97X-D	MP2	SCS-MP2
			Dimers		
Ben_2	−37.63 (−39.84)	−38.57 (−40.48)	−36.42 (−38.43)	−34.14	−31.70
$Naph_2$	−44.34 (−45.87)	−43.94 (−44.10)	−42.16 (−43.08)	−38.47	−36.53
Ant_2	−51.95 (−53.35)	−50.14 (−50.68)	−51.48 (−52.04)		
$Phen_2$	−47.68 (−48.37)	−46.02 (−46.63)	−49.27 (−51.36)		
Tet_2	−52.32 (−54.07)	−51.82 (−52.17)	−52.05 (−54.37)		
Pyr_2	−46.29 (−48.07)	−44.18 (−44.63)	−47.06 (−48.21)		
Cor_2	−60.13 (−62.38)	−55.11 (−56.38)	−56.53 (−59.35)		
			Trimers		
Ben_3	−79.39 (−78.92)	−68.35 (−62.42)	−73.15 (−78.98)	−67.92	−64.16
$Naph_3$	−94.62 (−96.35)	−84.86 (−81.92)	−87.64 (−90.97)		
Ant_3	−100.65 (−105.84)	−92.60 (−87.44)	−100.75 (−103.87)		
$Phen_3$	−89.51 (−77.39)	−86.12 (−74.81)	−87.89 (−89.54)		
Tet_3	−101.85 (−117.22)	−94.85 (−102.45)	−101.39 (−102.74)		
Pyr_3	−86.43 (−83.18)	−86.97 (−78.07)	−88.24 (−88.63)		
Cor_3	−121.14 (−113.31)	−115.15 (−115.36)	−117.62 (−118.06)		
			Tetramers		
Ben_4	−125.61	−114.37	−118.35		
$Naph_4$	−145.33	−133.76	−140.69		
Ant_4	−161.16	−143.99	−145.18		
$Phen_4$	−125.65	−111.50	−117.34		
			Pentamers		
Ben_5	−144.58	−137.49	−139.93		
$Naph_5$	−182.35	−167.48	−171.62		
Ant_5	−217.08	−193.60	−198.48		
$Phen_5$	−177.33	−150.39	−154.38		

[a]The results in chloroform solvent modeled using CPCM are listed in parentheses.

SCS-MP2, whereas the B3LYP-DCP functional underestimates the aggregation interaction enthalpy. The best agreement with the SCS-MP2 interaction enthalpy is calculated using the MP2 method (−0.28 kcal·mol^{-1} for Ben_2, −0.31 kcal·mol^{-1} for $Naph_2$, and −0.25 kcal·mol^{-1} for Ben_3), followed by the B3LYP-DCP (0.36 kcal·mol^{-1} for Ben_2, 0.09 kcal·mol^{-1} for $Naph_2$, and 0.46 kcal·mol^{-1} for Ben_3), B97D (−0.37 kcal·mol^{-1} for Ben_2, −0.42 kcal·mol^{-1} for $Naph_2$, and 1.60 kcal·mol^{-1} for Ben_3), and ωB97X-D functionals (−0.55 kcal·mol^{-1} for Ben_2, −0.87 kcal·mol^{-1} for $Naph_2$, and −1.12 kcal·mol^{-1} for Ben_3). Both B97D3 and M06-2X yield more negative interaction enthalpies for Ben_2 and $Naph_2$ than the reference SCS-MP2 method and the B97D and wB97X-D functionals (Supporting Information Table S2). The semiempirical PM6-DH2 method yields large nonsystematic deviations relative to SCS-MP2 (−1.5 kcal·mol^{-1} for Ben_2, 2.96 kcal·mol^{-1} for $Naph_2$, and −2.60 kcal·mol^{-1} for Ben_3) in addition to the structural distortions in longer π-stacked aggregates (Table 1, note *a*).

In Figure 3, we present the dependence of the enthalpy of π−π stacking interaction on the number of monomers of benzene, naphthalene, anthracene, and phenanthrene, calculated using the ωB97X-D functional. From the linear fitting slope, it is calculated that the tri-, tetra-, and pentamerization enthalpies are 2, 3, and 4 times as large as the dimerization enthalpy, respectively. Overall, the interaction between two PAH sheets does not reduce the ability of the aromatic system to further interact with successive PAH sheets. Our results indicate that the enthalpy of successive π−π stacking of PAHs, one over another, is rather constant and leads to aggregation. For comparison, we also included the π−π stacking interaction enthalpy of benzene dimer and trimer calculated using the SCS-MP2 method and found that the slope is in close agreement with that calculated using the ωB97X-D functional. It is important to note that the SCS-MP2 calculations have very high computational cost. The linear fitting analysis results are listed in Table 5.

In Figure 4, we show the linear dependence of the dimerization and trimerization enthalpies on the number of aromatic rings of the PAHs, calculated using the ωB97X-D functional. The linear fitting analysis results are listed in Table 5. The slopes of −3.7 and −7.2 kcal·mol^{-1} for dimerization and trimerization, respectively, give the enthalpy contribution of one benzene ring and indicate that the trimerization enthalpy is approximately twice as large as the dimerization enthalpy. The two groups of PAHs (linear and round) identified by the interplanar distances are also notable in this plot, especially for trimers of PAHs containing three and four fused rings. The interaction enthalpies of the linear PAHs are more negative than these of round PAHs, due to the larger bonding overlap area in linear than in round PAHs.

It is very important to consider the basis set superposition error for the dispersion-corrected methods, which may be calculated using the counterpoise (CP) correction procedure.[94,95] In the CP method, the BSSE is calculated by reperforming the monomer PES calculation with the same number of basis set of the dimer and then, comparing it with the PES of the uncorrected method.[96] The average CP corrections calculated using different functionals are 0.58 and 1.22 kcal·mol^{-1} (benzene), 1.25 and 2.58 kcal·mol^{-1} (naphthalene), 1.82 and 3.89 kcal·mol^{-1} (anthracene), 1.93 and 4.30

dx.doi.org/10.1021/jp408005h | J. Phys. Chem. A 2014, 118, 896−908

Table 4. Gibbs Free Energy (ΔG^{298}) in kcal·mol^{-1} (Eq 3) for the Dimers, Trimers, Tetramers, and Pentamers of Benzene (Ben), Naphthalene (Naph), Anthracene (Ant), Phenanthrene (Phen), Tetracene (Tet), Pyrene (Pyr), and Coronene (Cor) in the Gas Phase[a]

	B3LYP-DCP	B97D	ωB97X-D	MP2	SCS-MP2
			Dimers		
Ben_2	9.47 (11.23)	9.02 (10.39)	8.20 (10.22)	7.79	7.34
$Naph_2$	9.10 (10.20)	8.47 (9.50)	7.49 (7.84)	6.95	6.68
Ant_2	7.71 (8.62)	7.29 (7.46)	5.40 (6.21)		
$Phen_2$	7.42 (7.86)	7.02 (7.23)	6.68 (6.98)		
Tet_2	4.90 (5.12)	2.85 (5.44)	2.44 (4.84)		
Pyr_2	3.40 (3.75)	2.38 (4.19)	1.44 (2.70)		
Cor_2	−7.91 (−2.38)	−4.38 (1.08)	−2.68 (−1.1)		
			Trimers		
Ben_3	19.78 (21.94)	17.63 (16.09)	16.34 (20.49)	15.65	14.78
$Naph_3$	19.14 (20.54)	15.65 (16.25)	13.93 (15.38)		
Ant_3	15.58 (18.18)	11.73 (12.17)	9.62 (12.80)		
$Phen_3$	15.48 (10.71)	11.32 (8.35)	10.83 (14.38)		
Tet_3	7.19 (14.82)	6.21 (10.41)	4.79 (6.01)		
Pyr_3	6.10 (6.42)	4.62 (5.12)	2.78 (3.89)		
Cor_3	−11.92 (3.09)	−9.10 (6.30)	−7.73 (−5.92)		
			Tetramers		
Ben_4	33.35	31.25	28.26		
$Naph_4$	23.17	22.05	18.01		
Ant_4	15.43	12.36	10.37		
$Phen_4$	11.28	7.01	6.70		
			Pentamers		
Ben_5	34.66	32.15	28.71		
$Naph_5$	28.42	25.86	20.12		
Ant_5	20.90	18.14	10.35		
$Phen_5$	17.10	8.36	6.43		

[a]The results in chloroform solvent modeled using CPCM are listed in parentheses.

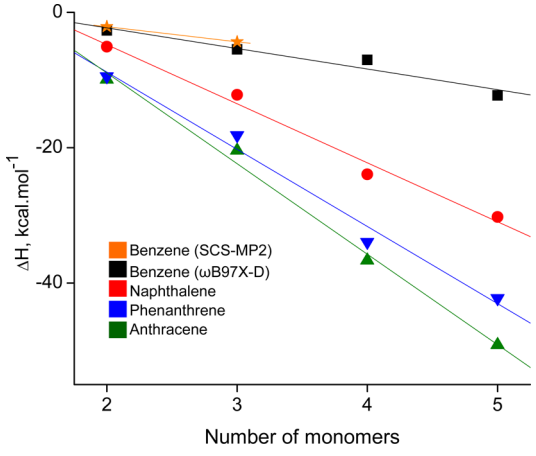

Figure 3. Enthalpy of $\pi-\pi$ stacking interaction calculated using the ωB97X-D functional plotted with respect to the number of PAH monomers in the gas phase. The SCS-MP2 results for benzene dimers and trimers in the gas phase are presented for comparison. The linear fitting results are shown as solid lines and are listed in Table 5.

kcal·mol^{-1} (phenanthrene), 2.75 and 5.52 kcal·mol^{-1} (tetracene), 2.38 and 5.10 kcal·mol^{-1} (pyrene), and 5.41 and 11.69 kcal·mol^{-1} (coronene) for the dimers and trimers, respectively. The CP corrections for MP2 and the SCS-MP2 are higher, with averages of 3.60 and 8.08 kcal·mol^{-1}, respectively, for benzene dimers (Supporting Information Table S3).

Entropy Analysis. An important thermodynamic quantity related to the $\pi-\pi$ stacking interaction is the entropy decrease due to the dimer, trimer, tetramer, and pentamer formation that at room temperature may dictate the aggregation process. The entropy is calculated as the sum of the electronic, translational, rotational, and vibrational motion contributions from each system component, as part of the frequency calculations. In Table 3, we list the entropy change for the aggregation of the PAHs and note that all dispersion-corrected functionals yield ΔS values substantially lower than the reference SCS-MP2 method, the ωB97X-D functional results being in the closest agreement. The results show that aggregation is disfavored for all the systems studied, as we are organizing larger systems.

In Figure 5, we present the dependence of aggregation entropy on the number of aromatic rings for dimers and trimers. We have two very distinct series of compounds: benzene, naphthalene, anthracene, and tetracene (linear) and phenanthrene and pyrene (round). These two groups have also been identified in the interplanar distance analysis and enthalpy subsections. The entropic penalty for organizing linear PAHs into dimer and trimer $\pi-\pi$ stacked aggregates is larger than for round PAHs by 7 and 13 cal·mol^{-1}, respectively, as evidenced by the intercept difference in Table 3. The distinction between linear and rounds PAHs is more pronounced in the entropy than in the enthalpy plots due to the larger entropic penalty to organize linear PAHs than that for round PAHs. It is important to note that the larger entropic penalty for linear PAHs is offset by the enthalpy gain.

Gibbs Free Energy Analysis. The ΔG^{298} values (Table 4) indicate that the aggregation of PAHs is not spontaneous at 298 K, except for coronene. In each set of dimers, trimers, tetramers, and pentamers, the ΔG^{298} values decrease as the number of aromatic rings in the aggregate is increased. The

dx.doi.org/10.1021/jp408005h | J. Phys. Chem. A 2014, 118, 896−908

Table 5. Linear Fitting Analysis Results for the Dependences of ΔH on the Number of Monomers (Figure 3) and Aromatic Rings (Figure 4), ΔS on the Number of Aromatic Rings (Figure 5), ΔG^{298} on the Number of Aromatic Rings (Figure 6), and Maximum Temperature for Aggregation (Figure 7) in the Gas Phase[a]

	slope, kcal·mol^{-1}	intercept, kcal·mol^{-1}	R^2
	Figure 3, ΔH		
benzene, SCS-MP2	−2.24	2.37	
benzene, ωB97X-D	−3.04	3.79	0.95
naphthalene, ωB97X-D	−8.72	12.66	0.99
phenanthrene, ωB97X-D	−11.41	13.98	0.98
anthracene, ωB97X-D	−13.38	17.80	0.99
	Figure 4, $\Delta H/\omega$B97X-D		
dimerization	−3.66 (−3.31)	1.54 (1.15)	0.99 (0.99)
trimerization	−7.19 (−7.16)	2.83 (3.59)	0.94 (0.97)
	Figure 5, $\Delta S/\omega$B97X-D		
dimers, linear[b]	−5.62 (−5.68)	−31.47 (−32.78)	0.77 (0.93)
dimers, round[b]	−2.58 (−3.10)	−38.11 (−37.24)	0.81 (0.92)
trimers, linear[b]	−9.78 (−8.42)	−66.27 (−73.10)	0.72 (0.80)
trimers, round[b]	−9.14 (−8.57)	−53.24 (−57.30)	0.98 (0.96)
	Figure 6, $\Delta G^{298}/\omega$B97X-D		
dimers	−1.95 (−1.88)	10.51 (11.63)	0.91 (0.95)
trimers	−4.17 (−4.56)	21.12 (25.24)	0.96 (0.95)
	Figure 7, T/ωB97X-D		
dimers and trimers	58.4 (54.5)	20.6 (16.6)	0.98 (0.98)

[a]The results for dimers and trimers in chloroform solvent modeled using CPCM are listed in parentheses. [b]In cal·mol^{-1}.

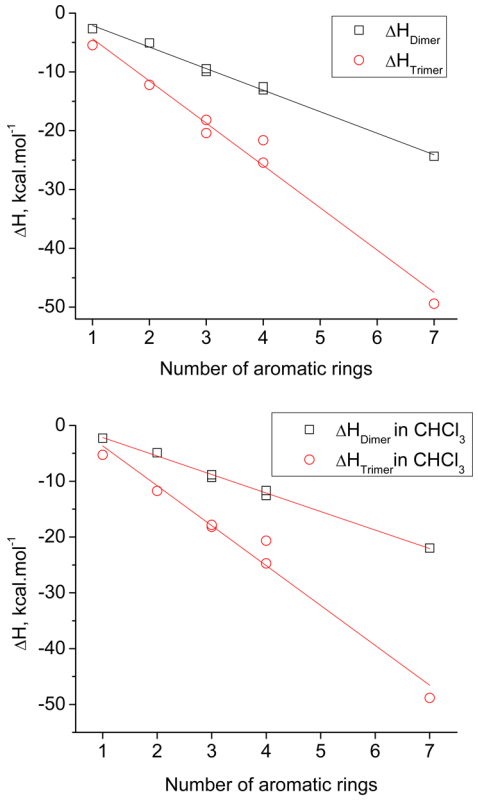

Figure 4. Dependence of the enthalpy of dimerization and trimerization on the number of fused aromatic rings in benzene, naphthalene, anthracene, tetracene, phenanthrene, pyrene, and coronene calculated using the ωB97X-D functional in the gas phase (top) and chloroform solvent modeled using CPCM (bottom). The linear fitting results are shown as solid lines and are listed in Table 5.

ΔG^{298} values for round PAHs are lower than these for linear PAHs, indicating that at 298 K the entropic contributions are larger than the enthalpic ones. Dimer formation is more favored than trimer and larger aggregate formation, with the exception of coronene, due to the entropic penalty. The ΔG^{298} values calculated using the ωB97X-D functional are in the closest agreement with the MP2 and SCS-MP2 results. The M06-2X yields ΔG^{298} of Pyr_3 that is substantially higher than than of Pyr_2. The B97D3 method yields negative ΔG^{298} for Tet_3, suggesting that this functional overestimates dispersion interactions (Supporting Information Table S4).

In Figure 6, we present the linear dependence of ΔG^{298} on the number of aromatic rings for dimer and trimer formation calculated using the ωB97X-D functional. The most important feature of this plot is the intersection at about five aromatic rings, indicating that PAHs containing less than five rings would form dimer aggregates, whereas PAHs containing more than five rings would form stable aggregates of three (or more) monomers. These predictions are in agreement with both the crystal structure of coronene that contains infinitely tall parallel stacks and the crystal structure of pyrene that contains dimers.[61,62] Smaller PAHs do not form parallel displaced-type π-stacked aggregates.[60] In Figure 7, we show the linear dependence of the maximum temperature (T^{max}) of spontaneous dimerization and trimerization of PAHs, calculated for $\Delta G^{298} = 0$ as $T^{max} = \Delta H/\Delta S$, on the number of fused rings in the PAHs. These results indicate that the dimers and trimers are stable under similar conditions and only aggregates containing five or more fused benzene rings, such as coronene, would form spontaneously at room temperature.

Effect of Chloroform Solvent on Thermochemistry. In Tables 2−4, we list in parentheses the interaction enthalpy, entropy, and ΔG^{298} for the PAHs calculated using the B3LYP-DCP, B97D, and ωB97X-D functionals coupled with the CPCM model to account for chloroform solvent. Our results show that the aggregation enthalpies become more negative as the size of the PAH system is increased, following the same trend as the gas phase results. The aggregation enthalpies in solution are about 10% higher relative to the gas phase, indicating weaker aggregation. The entropy in chloroform is more negative than that in the gas phase, indicating weaker aggregation. The Gibbs free energies at 298 K are higher in chloroform than in the gas phase, predicting weaker aggregation. It is very important to examine the performance of the three dispersion-corrected functionals with respect to the ΔG^{298} values calculated in chloroform solvent. The ΔG^{298} values calculated using the ωB97X-D functional in chloroform decrease as the aggregate size is increased and are negative for dimers and trimers of coronene, indicating spontaneous aggregation at 298 K. The ΔG^{298} values for coronene trimers calculated using the B3LYP-DCP and B97D functionals are positive, suggesting that coronene aggregation is not spontaneous in chloroform solvent. A discrepancy of B3LYP-DCP with both ωB97X-D and experimental results in terms of the order of increasing ΔG^{298} values has been noted for supramolecular asphaltene aggregates containing pyrene

dx.doi.org/10.1021/jp408005h | J. Phys. Chem. A 2014, 118, 896−908

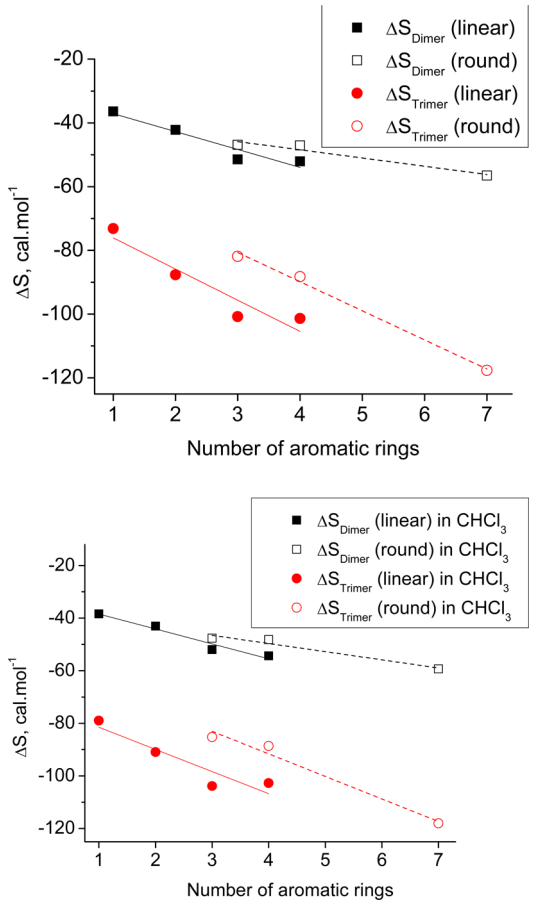

Figure 5. Dependence of the entropy of dimerization (ΔS) and trimerization on the number of fused aromatic rings in benzene, naphthalene, anthracene, tetracene, phenanthrene, pyrene, and coronene calculated using the ωB97X-D functional in the gas phase (top) and chloroform solvent modeled using CPCM (bottom). The linear fitting results are shown as solid and dashed lines for the linear and round PAHs and are listed in Table 5.

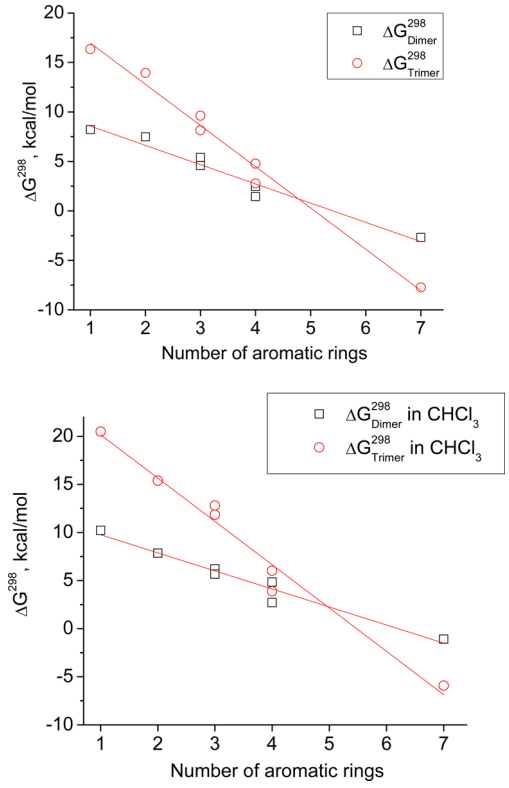

Figure 6. Gibbs free energy at 298 K for dimerization ($\Delta G^{298}_{\text{dimer}}$) and trimerization ($\Delta G^{298}_{\text{trimer}}$) of the PAHs benzene, naphthalene, anthracene, tetracene, phenanthrene, pyrene, and coronene, calculated using the ωB97X-D functional in the gas phase (top) and chloroform solvent modeled using CPCM (bottom). The linear fitting results are shown as solid lines and are listed in Table 5.

moieties.[43] This discrepancy could be attributed to incompatibility between the dispersion correction for C atoms and the CPCM solvation model. The ωB97X-D functional predicts the thermodynamics of aggregation in a very good agreement with experimental results.

In Figures 3−7, we also present the linear dependences of enthalpy, entropy, and ΔG^{298} on the number of benzene rings in PAHs calculated using the ωB97X-D/CPCM method. The correlations between thermochemistry results in solution and the gas phase calculated using the ωB97X-D functional are highlighted by the agreement of the linear fitting analysis results listed in Table 5.

CONCLUSIONS

Ab initio, DFT, and semiempirical methods, with and without dispersion correction, are employed to study the π-stacking aggregation of PAHs. The interplanar distances, aggregation enthalpies, entropies, and ΔG^{298} are calculated and compared with the accurate SCS-MP2 method selected as a reference. The MP2 thermochemistry results are in the closest agreement with SCS-MP2, but both of these methods have very high computational cost. Our results show that widely used DFT functionals and semiempirical methods do not provide adequate prediction of geometry and thermochemistry for $\pi-\pi$ stacking interactions of PAHs. The semiempirical PM6-DH2 method yields distorted stacks of PAHs and non-systematic deviations in thermochemistry.

Among the dispersion-corrected DFT methods, the DFT-D functionals B97D and ωB97X-D with augmented damped R^{-6} dispersion term predict longer $\pi-\pi$ stacking distances than the reference SCS-MP2 method, whereas the B3LYP-DCP functional predicts very short distances. The dispersion-corrected functionals predict the same trend of decreasing interaction enthalpy and entropy as both the PAH size and the number of monomers in the aggregate are increased. The B97D and ωB97X-D functionals yield more negative interaction enthalpies and entropies than the SCS-MP2, whereas the B3LYP-DCP functional yields less negative enthalpies. Among the DFT methods with dispersion correction, the ωB97X-D functional provides the most accurate prediction of interplanar distances and thermodynamics at a reasonable computational cost, making it attractive for the prediction of π-stacking and aggregation interactions in systems of relevance, such as molecular asphaltene aggregates. In chloroform solvent described using the CPCM method, only the ωB97X-D functional predicts correctly the spontaneous formation of coronene dimer and trimer aggregates. It is important to note that the computational cost of ωB97X-D, B97D, and B97D3 calculations is less than half the cost of B3LYP-DCP and M062X calculations. The B3LYP-DCP and B97D functionals should be used cautiously for prediction of aggregation thermochemistry in continuum solvent. These and previous results[43] make the ωB97X-D functional both accurate and

dx.doi.org/10.1021/jp408005h | J. Phys. Chem. A 2014, 118, 896−908

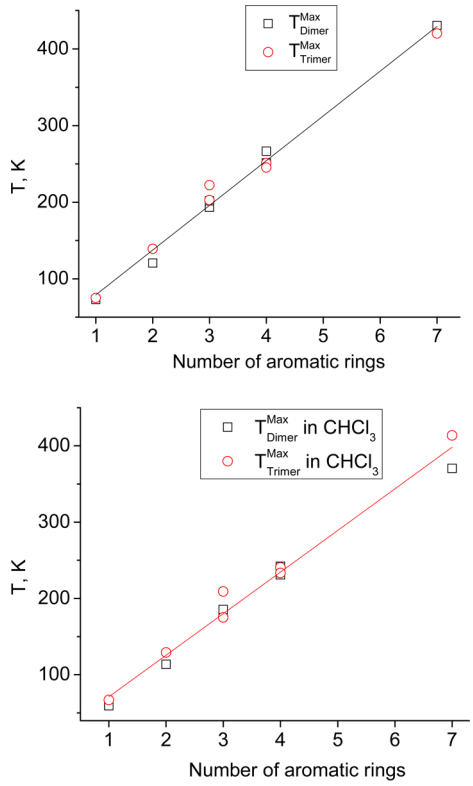

Figure 7. Maximum temperature for spontaneous dimer (T^{max}_{dimer}) and trimer (T^{max}_{dimer}) aggregation ($\Delta G^{298} < 0$) calculated as $T^{max} = \Delta H/\Delta S$ based on the enthalpy and entropy results from the ωB97X-D functional in the gas phase (top) and chloroform solvent modeled using CPCM (bottom). The linear fitting results are shown as solid lines and are listed in Table 5.

efficient for prediction of the important π-stacking and hydrogen bonding contributions to intermolecular aggregation interactions of asphaltenes in solution.

We employ the ωB97X-D functional to analyze the enthalpy, entropy, and ΔG^{298} for aggregation of PAHs in the gas phase as well as in chloroform solvent represented using the CPCM method. The results show that the aggregation enthalpy of PAHs increases linearly as the number of fused rings and PAH monomers in the aggregate are increased. The aggregation entropy is negative and decreases as the PAH system size is increased. For the two distinct types of PAHs (linear and round) the entropic penalty to form $\pi-\pi$ stacked aggregates is larger for the round ones, whereas the enthalpic stabilization is larger for the linear ones. The overall effect on ΔG^{298} is that aggregates of round (carbon-rich) PAHs are more stable at room temperature. On the basis of ΔG^{298} results linear fitting, we predict that PAHs containing more than five fused rings, such as coronene, would aggregate spontaneously at 298 K. We also predict that PAHs containing more than five fused rings would spontaneously form aggregates containing three (or more) monomers stacked in a parallel displaced configuration. The ΔG^{298} of pyrene is slightly positive, suggesting that pyrene would form dimers close to room temperature. The ωB97X-D results in chloroform highlight the same trends and do not differ significantly from gas phase results. These computational results are in agreement with X-ray crystallographic determinations that show the formation of infinitely long parallel stacks of coronene, the formation of dimers of pyrene, and the lack of parallel stacking in smaller and linear PAHs. This investigation provides insight into dispersion interactions and aggregation of systems containing PAHs and would help guide the synthesis of asphaltene model compounds[37,38] toward understanding intermolecular interactions in heavy petroleum.[42,43]

■ ASSOCIATED CONTENT

Supporting Information

Tables of interplanar distances, dispersion interaction enthalpies, BSSEs, Gibbs free energies, and Cartesian coordinates. This material is available free of charge via the Internet at http://pubs.acs.org.

■ AUTHOR INFORMATION

Corresponding Authors

*J. Walkimar de M. Carneiro: e-mail, walk@vm.uff.br.

*A. Kovalenko: e-mail, andriy.kovalenko@nrc-cnrc.gc.ca.

Notes

The authors declare no competing financial interest.

■ ACKNOWLEDGMENTS

This work was supported by the National Institute for Nanotechnology and the University of Alberta. L. M. da Costa acknowledges his graduate fellowship from Fundação Carlos Chagas Filho de Amparo à Pesquisa (FAPERJ) (Proc. E-26/152.786/2006). S. R. Stoyanov, S. Gusarov, and A. Kovalenko acknowledge the financial support of the Imperial Oil–Alberta Innovates Energy and Environment Solutions Centre for Oil Sands Innovation (COSI) at the University of Alberta. J. W. de M. Carneiro received a research grant from Conselho Nacional de Desenvolvimento Científico e Tecnológico (CNPq-Brazil). S. R. Stoyanov thanks Dr. John M. Villegas for his discussion and suggestions on the presentation of the results. The authors acknowledge the assistance of Dr. Robert McDonald of the X-Ray Crystallography Laboratory in the Department of Chemistry at the University of Alberta with the access to the Cambridge Structural Database. The high performance computing resources were provided by WestGrid–Compute/Calcul Canada.

■ REFERENCES

(1) Chalasinski, G.; Szczesniak, M. M. State of the Art and Challenges of the Ab initio Theory of Intermolecular Interactions. *Chem. Rev.* **2000**, *100*, 4227–4252.

(2) Kozmon, S.; Matuska, R.; Spiwok, V.; Koca, J. Dispersion Interactions of Carbohydrates with Condensate Aromatic Moieties: Theoretical Study on the CH-pi Interaction Additive Properties. *Phys. Chem. Chem. Phys.* **2011**, *13*, 14215–14222.

(3) Antony, J.; Grimme, S.; Liakos, D. G.; Neese, F. Protein-Ligand Interaction Energies with Dispersion Corrected Density Functional Theory and High-Level Wave Function Based Methods. *J. Phys. Chem. A* **2011**, *115*, 11210–11220.

(4) Lanzarotti, E.; Biekofsky, R. R.; Estrin, D. A.; Marti, M. A.; Turjanski, A. G. Aromatic-Aromatic Interactions in Proteins: Beyond the Dimer. *Chem. Inf. Model.* **2011**, *51*, 1623–1633.

(5) Sun, W.; Bu, Y. On the Binding Strength Sequence for Nucleic Acid Bases and C-60 with Density Functional and Dispersion-Corrected Density Functional Theories: Whether C-60 Could Protect Nucleic Acid Bases from Radiation-Induced Damage. *J. Phys. Chem. C* **2011**, *115*, 3220–3228.

(6) Maschio, L.; Civalleri, B.; Ugliengo, P.; Gavezzotti, A. Intermolecular Interaction Energies in Molecular Crystals: Comparison and Agreement of Localized Moller-Plesset 2, Dispersion-Corrected Density Functional, and Classical Empirical Two-Body Calculations. *J. Phys. Chem. A* **2011**, *115*, 11179–11186.

(7) Ehrlich, S.; Moellmann, J.; Grimme, S. Dispersion-Corrected Density Functional Theory for Aromatic Interactions in Complex Systems. *Acc. Chem. Res.* **2013**, *46*, 916−926.
(8) Li, S.; Cooper, V. R.; Thonhauser, T.; Lundqvist, B. I.; Langreth, D. C. Stacking Interactions and DNA Intercalation. *J. Phys. Chem. B* **2009**, *113*, 11166−11172.
(9) Dobson, J. F. Dispersion and Induction Interactions of Graphene with Nanostructures. *Surf. Sci.* **2011**, *605*, 1621−1632.
(10) Aravinda, S.; Shamala, N.; Das, C.; Sriranjini, A.; Karle, I. L.; Balaram, P. Aromatic-Aromatic Interactions in Crystal Structures of Helical Peptide Scaffolds Containing Projecting Phenylalanine Residues. *J. Am. Chem. Soc.* **2003**, *125*, 5308−5315.
(11) Strausz, O. P.; Lown, E. M. *The Chemistry of Alberta Oil Sands Bitumens and Heavy Oils*; AERI: Calgary, AB, 2003.
(12) Tsuzuki, S.; Lüthi, H. P. Interaction Energies of van der Waals and Hydrogen Bonded Systems Calculated Using Density Functional Theory: Assessing the PW91 Model. *J. Chem. Phys.* **2001**, *114*, 3949−3957.
(13) Hohenstein, E. G.; Jaeger, H. M.; Carrell, E. J.; Tschumper, G. S.; Sherrill, C. D. Accurate Interaction Energies for Problematic Dispersion-Bound Complexes: Homogeneous Dimers of NCCN, P-2, and PCCP. *J. Chem. Theory Comput.* **2011**, *7*, 2842−2851.
(14) Burns, L. A.; Vázquez-Mayagoitia, Á.; Sumpter, B. G.; Sherrill, C. D. Density-Functional Approaches to Noncovalent Interactions: A Comparison of Dispersion Corrections (DFT-D), Exchange-Hole Dipole Moment (XDM) Theory, and Specialized Functionals. *J. Chem. Phys.* **2011**, *134*, 84107-1−84107-25.
(15) Grimme, S.; Ehrlich, S.; Goerigk, L. Effect of the Damping Function in Dispersion Corrected Density Functional Theory. *J. Comput. Chem.* **2011**, *32*, 1456−1465.
(16) Sinnokrot, M. O.; Sherrill, C. D. High-Accuracy Quantum Mechanical Studies of pi-pi Interactions in Benzene Dimers. *J. Phys. Chem. A* **2006**, *110*, 10656−10668.
(17) Geng, Y.; Takatani, T.; Hohenstein, E. G.; Sherrill, C. D. Accurately Characterizing the pi-pi Interaction Energies of Indole-Benzene Complexes. *J. Phys. Chem. A* **2010**, *114*, 3576−3582.
(18) Roothaan, C. C. J. New Developments in Molecular Orbital Theory, Self-Consistent Orbitals for Radicals, Self-Consistent Perturbation Theory. *Rev. Mod. Phys.* **1951**, *23*, 69−89.
(19) Pople, J. A.; Nesbet, R. K. Perturbation theory. *J. Chem. Phys.* **1954**, *22*, 571−572.
(20) McWeeny, R.; Dierksen, G. Extension to Open Shells. *J. Chem. Phys.* **1968**, *49*, 4852−4856.
(21) Tsuzuki, S.; Honda, K.; Uchimaru, T.; Mikami, M.; Tanabe, K. Origin of Attraction and Directionality of the x/x Interaction: Model Chemistry Calculations of Benzene Dimer Interaction. *J. Am. Chem. Soc.* **2002**, *124*, 104−112.
(22) Hobza, P.; Spooner, J.; Reschel, T. Density-Functional Theory and Molecular Clusters. *J. Comput. Chem.* **1995**, *16*, 1315−1325.
(23) Head-Gordon, M.; Pople, J. A.; Frisch, M. J. MP2 Energy Valuation by Direct Methods, Avoiding the Integral Storage Bottleneck in LCAO Calculations in Electron Correlation. *Chem. Phys. Lett.* **1988**, *153*, 503−506.
(24) Saebø, S.; Almlöf, J. A Direct MP2 Gradient-Method. *Chem. Phys. Lett.* **1989**, *154*, 83−89.
(25) Frisch, M. J.; Head-Gordon, M.; Pople, J. A. Semidirect Algorithms for the MP2 Energy and Gradients. *Chem. Phys. Lett.* **1990**, *166*, 275−280.
(26) Frisch, M. J.; Head-Gordon, M.; Pople, J. A. Analytic MP2 Frequencies Without Fifth-Order Storage. *Chem. Phys. Lett.* **1990**, *166*, 281−289.
(27) Head-Gordon, M.; Head-Gordon, T. Theory and Application to Bifurcated Hydrogen Bonds in the Water Hexamer. *Chem. Phys. Lett.* **1994**, *220*, 122−128.
(28) Hobza, P.; Selzle, H. L.; Schlag, E. W. Potential Energy Surface for the Benzene Dimer. Results of Ab initio CCSD(T) Calculations Show Two Nearly Isoenergetic Structures: T-shaped and Parallel-Displaced. *J. Phys. Chem.* **1996**, *100*, 18790−18794.
(29) Sinnokrot, M. O.; Valeev, E. F.; Sherrill, C. D. Estimates of the Ab initio Limit for pi-pi Interactions: The Benzene Dimer. *J. Am. Chem. Soc.* **2002**, *124*, 10887−10893.
(30) Purvis, G. D.; Bartlett, R. J. A Bull Coupled-Cluster Singles and Doubles Model − The Inclusion of Disconnected Triples. *J. Chem. Phys.* **1982**, *76*, 1910−1918.
(31) Hopkins, B. W.; Tschumper, G. S. Ab initio Studies of pi-pi Interactions: The Effects of Quadruple Excitations. *J. Phys. Chem. A* **2004**, *108*, 2941−2948.
(32) Grimme, S. Accurate Description of van der Waals Complexes by Density Functional Theory Including Empirical Corrections. *J. Comput. Chem.* **2004**, *25*, 1464−1473.
(33) Mackie, I. D.; DiLabio, G. Interactions in Large, Polyaromatic Hydrocarbon Dimers: Application of Density Functional Theory with Dispersion Corrections. *J. Phys. Chem. A* **2008**, *112*, 10968−10976.
(34) Torres, E.; DiLabio, G. A. A (Nearly) Universally Applicable Method for Modeling Noncovalent Interactions Using B3LYP. *J. Phys. Chem. Lett.* **2012**, *3*, 1738−1744.
(35) Chai, J.-D.; Head-Gordon, M. Long-Range Corrected Hybrid Density Functionals with Damped Atom-Atom Dispersion Corrections. *Phys. Chem. Chem. Phys.* **2008**, *10*, 6615−6620.
(36) Grimme, S. Density Functional Theory with London Dispersion Corrections. *Wiley Interdisc. Rev. Comput. Mol. Sci.* **2011**, *1*, 211−228.
(37) Rezac, J.; Fanfrlık, J.; Salahub, D.; Hobza, P. Semiempirical Quantum Chemical PM6Method Augmented by Dispersion and H-Bonding Correction Terms Reliably Describes Various Types of Noncovalent Complexes. *J. Chem. Theory Comput.* **2009**, *5*, 1749−1760.
(38) Grimme, S. Improved Second-Order Moller-Plesset Perturbation Theory by Separate Scaling of Parallel- and Antiparallel-Spin Pair Correlation Energies. *J. Chem. Phys.* **2003**, *118*, 9095−9102.
(39) Takatani, T.; Hohenstein, E. G.; Sherrill, C. D. Improvement of the Coupled-Cluster Singles and Doubles Method via Scaling Same- and Opposite-Spin Components of the Double Excitation Correlation Energy. *J. Chem. Phys.* **2008**, *128*, 124111-1−124111-7.
(40) Hill, J. G.; Platts, J. A. Spin-Component Scaling Methods for Weak and Stacking Interactions. *J. Chem. Theory Comput.* **2007**, *3*, 80−85.
(41) Distasio, R. A., Jr.; Head-Gordon, M. Optimized Spin-Component Scaled Second-Order Moller-Plesset Perturbation Theory for Intermolecular Interaction Energies. *Mol. Phys.* **2007**, *105*, 1073−1083.
(42) Hesselmann, A. Improved Supermolecular Second Order Moller-Plesset Intermolecular Interaction Energies Using Time-Dependent Density Functional Response Theory. *J. Chem. Phys.* **2008**, *128*, 144112-1−144112-9.
(43) Jansen, G.; Hesselmann, A. Comment on "Using Kohn-Sham Orbitals in Symmetry-Adapted Perturbation Theory to Investigate Intermolecular Interactions". *J. Phys. Chem. A* **2001**, *105*, 11156−11157.
(44) Hesselmann, A.; Jansen, G.; Schutz, M. Density-Functional Theory-Symmetry-Adapted Intermolecular Perturbation Theory with Density Fitting: A New Efficient Method to Study Intermolecular Interaction Energies. *J. Chem. Phys.* **2005**, *122*, 014103-1−014103-17.
(45) Szalewicz, K.; Patkowski, K.; Jeziorski, B. Intermolecular Interactions via Perturbation Theory: From Diatoms to Biomolecules. *Struct. Bonding (Berlin)* **2005**, *116*, 43−117.
(46) Groenzin, H.; Mullins, O. C ·molecular Size and Structure of Asphaltenes from Various Sources. *Energy Fuels* **2000**, *14*, 677−684.
(47) Strausz, O. P.; Peng, P.; Murgich, J. About the Colloidal Nature of Asphaltenes and the MW of Covalent Monomeric Units. *Energy Fuels* **2002**, *16*, 809−822.
(48) Strausz, O. P.; Mojelsky, T. W.; Lown, E. M. The Molecular-Structure of Asphaltene − an Unfolding Story. *Fuel* **1992**, *71*, 1355−1363.
(49) Tan, X.; Fenniri, H.; Gray, M. R. Pyrene Derivatives of 2,2′-bipyridine as Models for Asphaltenes: Synthesis, Characterization, and Supramolecular Organizations. *Energy Fuels* **2008**, *22*, 715−720.

(50) Tan, X.; Fenniri, H.; Gray, M. R. Water Enhances the Aggregation of Model Asphaltenes in Solution via Hydrogen Bonding. *Energy Fuels* **2009**, *23*, 3687−3693.
(51) Takanohashi, T.; Lino, M.; Nakamura, K. Evaluation of Association of Solvent-Soluble Molecules of Bituminous Coal by Computer Simulation. *Energy Fuels* **1994**, *8*, 395−398.
(52) Takanohashi, T.; Lino, M.; Nakamura, K. Simulation of Interaction of Coal Associates with Solvents Using the Molecular Dynamics Calculation. *Energy Fuels* **1998**, *12*, 1168−1173.
(53) Murgich, J ·molecular Simulation and the Aggregation of the Heavy Fractions in Crude Oils. *Mol. Simul.* **2003**, *29*, 451−461.
(54) Murgich, J. Intremolecular Forces in Aggregates of Asphaltenes and Resins. *Pet. Sci. Technol.* **2002**, *20*, 983−997.
(55) Murgich, J.; Rodrigues, J. M.; Aray, Y ·molecular Recognition and Molecular Mechanics of Micelles of Some Model Asphaltenes and Resins. *Energy Fuels* **1996**, *10*, 68−76.
(56) Gray, M. R.; Tykwinski, R.; Stryker, J. M.; Tan, X. Supramolecular Assembly Model for Aggregation of Petroleum Asphaltenes. *Energy Fuels* **2011**, *25*, 3125.
(57) Costa, L. M.; Stoyanov, S. R.; Gusarov, S.; Tan, X.; Gray, M. R.; Stryker, J. M.; Tykwinski, R.; Carneiro, J. W. M.; Seidl, P. R.; Kovalenko, A. Density Functional Theory Investigation of the Contributions of pi-pi Stacking and Hydrogen-Bonding Interactions to the Aggregation of Model Asphaltene Compounds. *Energy Fuels* **2012**, *26*, 2727−2735.
(58) Costa, L. M.; Hayaki, S.; Stoyanov, S. R.; Gusarov, S.; Tan, X.; Gray, M. R.; Stryker, J. M.; Tykwinski, R.; Carneiro, J. W. M.; Sato, H.; Seidl, P. R.; Kovalenko, A. 3D-RISM-KH Molecular Theory of Solvation and Density Functional Theory Investigation of the Role of Water in the Aggregation of Model Asphaltenes. *Phys. Chem. Chem. Phys.* **2012**, *14*, 3922−3934.
(59) A. Kovalenko. Three-dimensional RISM Theory for Molecular Liquids And Solid-Liquid Interfaces. In: *Molecular Theory of Solvation: Understanding Chemical Reactivity*; Hirata, F., Ed.; Kluwer Academic Publishers: Dordrecht Netherlands, 2003; pp 169−275.
(60) Kovalenko, A.; Hirata, F. Self-Consistent Description of a Metal-Water Interface by the Kohn-Sham Density Functional Theory and the Three-Dimensional Reference Interaction Site Model. *J. Chem. Phys.* **1999**, *110*, 10095−10112.
(61) Kovalenko, A.; Hirata, F. Potentials of Mean Force of Simple Ions in Ambient Aqueous Solution. I. Three-Dimensional Reference Interaction Site Model Approach. *J. Chem. Phys.* **2000**, *112*, 10391−10417.
(62) Gusarov, S.; Pujari, B. S; Kovalenko, A. Efficient Treatment of Solvation Shells in 3D Molecular Theory of Solvation. *J. Comput. Chem.* **2012**, *33*, 1478−1494.
(63) Grimme, S.; Goerigk, L.; Fink, R. F. Spin-Component-Scaled Electron Correlation Methods. *WIREs Comput. Mol. Sci* **2012**, *2*, 886−906.
(64) Frisch, M. J.; Trucks, G. W.; Schlegel, H. B.; Scuseria, G. E.; Robb, M. A.; Cheeseman, J. R.; Scalmani, G.; Barone, V.; Mennucci, B.; Petersson, G. A.; Nakatsuji, H.; Caricato, M.; Li, X.; Hratchian, H. P.; Izmaylov, A. F.; Bloino, J.; Zheng, G.; Sonnenberg, J. L.; Hada, M.; Ehara, M.; Toyota, K.; Fukuda, R.; Hasegawa, J.; Ishida, M.; Nakajima, T.; Honda, Y.; Kitao, O.; Nakai, H.; Vreven, T.; Montgomery, J. A., Jr.; Peralta, J. E.; Ogliaro, F.; Bearpark, M.; Heyd, J. J.; Brothers, E.; Kudin, K. N.; Staroverov, V. N.; Kobayashi, R.; Normand, J.; Raghavachari, K.; Rendell, A.; Burant, J. C.; Iyengar, S. S.; Tomasi, J.; Cossi, M.; Rega, N.; Millam, N. J.; Klene, M.; Knox, J. E.; Cross, J. B.; Bakken, V.; Adamo, C.; Jaramillo, J.; Gomperts, R.; Stratmann, R. E.; Yazyev, O.; Austin, A. J.; Cammi, R.; Pomelli, C.; Ochterski, J. W.; Martin, R. L.; Morokuma, K.; Zakrzewski, V. G.; Voth, G. A.; Salvador, P.; Dannenberg, J. J.; Dapprich, S.; Daniels, A. D.; Farkas, Ö.; Foresman, J. B.; Ortiz, J. V.; Cioslowski, J.; Fox, D. J. *Gaussian 09*, Revision A.1; Gaussian, Inc.: Wallingford, CT, 2009.
(65) Becke, A. D. Density-Functional Thermochemistry. 1. The Effect of the Exchange-Only Gradient Correction. *J. Chem. Phys.* **1992**, *96*, 2155−2160.
(66) Lee, C.; Yang, W.; Parr, R. G. Development of the Colle-Slavetti Correlation-Energy Formula into a Functional of the Electron-Density. *Phys. Rev. B* **1988**, *37*, 785−789.
(67) (a) Perdew, J. P.; Burke, K.; Ernzerhof, M. Generalized Gradient Approximation Made Simple. *Phys. Rev. Lett.* **1996**, *77*, 3865−3868.
(68) Perdew, J. P.; Burke, K.; Ernzerhof, M. Errata: Generalized Gradient Approximation Made Simple. *Phys. Rev. Lett.* **1997**, *78*, 1396−1396.
(69) Yanai, T.; Tew, D.; Handy, N. A New Hybrid Exchange-Correlation Functional Using the Coulomb-Attenuating Method (CAM-B3LYP). *Chem. Phys. Lett.* **2004**, *393*, 51−57.
(70) Tawada, Y.; Tsuneda, T.; Yanagisawa, S.; Yanai, T.; Hirao, K. A Long-Range-Corrected Time-Dependent Density Functional Theory. *J. Chem. Phys.* **2004**, *120*, 8425−8433.
(71) Vydrov, O. A.; Scuseria, G. E. Assessment of a Long-Range Corrected Hybrid Functional, Importance of Short-Range Versus Long-Range Hartree-Fock Exchange for the Performance of Hybrid Density Functionals. *J. Chem. Phys.* **2006**, *125*, 234109−1−234109−9.
(72) Vydrov, O. A.; Heyd, J.; Krukau, A.; Scuseria, G. E. Importance of Short-Range Versus Long-Range Hartree-Fock Exchange for the Performance of Hybrid Density Functionals. *J. Chem. Phys.* **2006**, *125*, 074106-1−074106-9.
(73) Vydrov, O. A.; Scuseria, G. E.; Perdew, J. P. Tests of Functionals for Systems with Fractional Electron Number. *J. Chem. Phys.* **2007**, *126*, 154109-1−154109-9.
(74) Grimme, S. Semiempirical GGA-Type Density Functional Constructed with a Long-Range Dispersion Correction. *J. Comput. Chem.* **2006**, *27*, 1787−1799.
(75) Grimme, G.; Ehrlich, S.; Goerigk, L. Effect of the Damping Function in Dispersion Corrected Density Functional Theory. *J. Comput. Chem.* **2011**, *32*, 1456−1465.
(76) Zhao, Y.; Truhlar, D. G. The M06 Suite of Density Functionals for Main Group Thermochemistry, Thermochemical Kinetics, Noncovalent Interactions, Excited States, and Transition Elements: Two New Functionals and Systematic Testing of Four M06-Class Functionals and 12 Other Functionals. *Theor. Chem. Acc.* **2008**, *120*, 215−41.
(77) Neese, F. *ORCA − an ab initio, Density Functional and Semiempirical Program Package*, Version 2.6; University of Bonn, 2008.
(78) Rassolov, V. A.; Ratner, M. A.; Pople, J. A.; Redfern, P. C.; Curtiss, L. A. 6-31G* basis set for third-row atoms. *J. Comput. Chem.* **2001**, *22*, 976−984.
(79) Frisch, M. J.; Pople, J. A.; Binkley, J. S. Self-Consistent Molecular-Orbital Methods. 25. Supplementary Functions for Gaussian-Basis Sets. *J. Chem. Phys.* **1984**, *80*, 3265−3269.
(80) Dewar, M. J. S.; Zoebisch, E. Z.; Healy, E. F.; Stewart, J.-D. The Development and Use pf Quantum-Mechanical Molecular-Models. 76. AM1 − a New Generatal-Purpuse Quantum-Mechanical Molecular-Model. *J. Am. Chem. Soc.* **1985**, *107*, 3902−3909.
(81) Stewart, J. J. P. Optimization of Parameters for Semiempirical Methods. *J. Comput. Chem.* **1989**, *10*, 209−220.
(82) Stewart, J. J. P. Optimization of Parameters for Semiempirical Methods V: Modification of NDDO Approximations and Application to 70 Elements. *J. Mol. Model.* **2007**, *13*, 1173−1213.
(83) Stewart, J. J. P. *MOPAC 2009*, Version DS-DG1; Stewart Computational Chemistry: Colorado Springs, CO, 2008.
(84) Barone, V.; Cossi, M. Quantum Calculation of Molecular Energies and Energy Gradients in Solution by a Conductor Solvent Model. *J. Phys. Chem. A* **1998**, *102*, 1995−1998.
(85) Cossi, M.; Rega, N.; Scalmani, G.; Barone, V. Energies, Structures, and Electronic Properties of Molecules in Solution with the C-PCM Solvation Model. *J. Comput. Chem.* **2003**, *24*, 669−674.
(86) Janowski, T.; Pulay, P.; Karunarathna, A. A. S.; Sygula, A.; Saebø, S. Convex-Concave Stacking of Curved Conjugated Networks: Benchmark Calculations on the Corannulene Dimer. *Chem. Phys. Lett.* **2011**, *512*, 155−160.
(87) Nayak, S. K.; Sathishkumar, R.; Row, T. N. G. Directing Role of Functional Groups in Selective Generation of C-H - Pi Interactions: In

Situ Cryo-Crystallographic Studies on Benzyl Derivatives. *Cryst. Eng. Commun.* **2010**, *12*, 3112−3118.
(88) Oddershede, J.; Larsen, S. Charge Density Study of Naphthalene Based on X-Ray Diffraction Data at Four Different Temperatures and Theoretical Calculations. *J. Phys. Chem. A* **2004**, *108*, 1057−1063.
(89) Brock, C. P.; Dunitz, J. D. Temperature-Dependence of Thermal Motion in Crystalline Anthracene. *Acta Crystallogr., Sect. B: Struct. Sci.* **1990**, *46*, 795−806.
(90) Petricek, V.; Cisarova, I.; Hummel, L.; Kroupa, J.; Brezina, B. Orientional Disorder in Phenanthrene − Structural Determination at 248-K 295-K, 339-K AND 344-K. *Acta Crystallogr., Sect. B: Struct. Sci.* **1990**, *46*, 830−832.
(91) Holmes, D.; Kumaraswamy, S.; Matzger, A. J.; Vollhardt, K. P. C. On the Nature of Nonplanarity in the [N]phenylenes. *Chem.—Eur. J.* **1999**, *5*, 3399−3412.
(92) Camerman, A.; Trotter, J. Crystal Molecular Structure of Pyrene. *Acta Crystallogr.* **1965**, *18*, 636−643.
(93) Fawcett, J. K.; Trotter, J. The Crystal and Molecular Structure of Coronene. *Proc. R. Soc. London, Ser. A* **1965**, *289*, 366−376.
(94) Boys, S. F.; Bernardi, F.; Boys, S. F.; Bernardi, F. Calculation of Small Molecular Interactions by Differences of Separate Total Energies − Some Procedures with Reduced Errors. *Mol. Phys.* **1970**, *19*, 553−566.
(95) Simon, S.; Duran, M.; Dannenberg, J. J. How Does Basis Set Superposition Error Change the Potential Surfaces for Hydrogen Bonded Dimers? *J. Chem. Phys.* **1996**, *105*, 11024−11031.
(96) van Duijneveldt, F. B.; van Duijneveldt, J. G. C. M.; van Lenthe, J. H. State-of-Art in Counterpoise Theory. *Chem. Rev.* **1994**, *94*, 1873−1885.